Eur. Phys. J. B **45**, 331–338 (2005)
DOI: 10.1140/epjb/e2005-00202-8

THE EUROPEAN PHYSICAL JOURNAL B

Magnetic nanoscale aggregates of cobalt and nickel in MgO single crystals

J.V. Pinto[1,2,3], M.M. Cruz[1,a], R.C. da Silva[2,4], E. Alves[2,4], R. González[5], and M. Godinho[1]

[1] Dep. de Física/CFMC-UL, FCUL, Campo Grande, Ed. C8, 1749-016 Lisboa, Portugal
[2] LFI, Dep. de Física, ITN, E.N.10 2686-953 Sacavém, Portugal
[3] Dep. de Física/FCT-UNL, Monte da Caparica, 2829-516 Caparica, Portugal
[4] CFNUL, Av. Prof. Gama Pinto 2, 1649-003 Lisboa, Portugal
[5] Dep. de Física, Universidad Carlos III, 28911 Leganés (Madrid), Spain

Received 3 March 2005 / Received in final form 11 April 2005
Published online 6 July 2005 –

Abstract. The magnetic properties of Co and Ni nanosized aggregates formed after implantation of nickel and cobalt ions in magnesium oxide single crystals were investigated. The influence of the implantation energy and annealing treatments was characterized. The particle size distribution was determined from the combined analysis of the magnetic moment dependence on both magnetic field and temperature, and used to determine the magnetic anisotropy constant of the aggregates. The results for nickel aggregates indicate the presence of an antiferromagnetic layer after the annealing treatments.

PACS. 75.50.Tt Fine-particle systems; nanocrystalline materials – 61.72.Ww Doping and impurity implantation in other materials – 75.50.Dd Nonmetallic ferromagnetic materials

1 Introduction

Semiconductors and oxides doped with magnetic ions are nowadays an increasingly important group of materials since they are good candidates for spin controlled transport. Included in this class of materials thin films of cobalt doped anatase were reported in 2001 as the first ferromagnetic semiconductor at room temperature [1]. The nucleation of cobalt rich magnetic particles was claimed to be associated with its ferromagnetic behaviour [2]. In the case of magnesium oxide, other new possibilities are opened if it can be endowed with magnetic properties. Magnesium oxide is an important material for optical applications and as such the existence of an ordered magnetic state can be used to control optical polarization effects. It is also important as a substrate for growing magnetic semiconductor and oxide films and, consequently, magnetically doped MgO may offer the possibility of acting as a magnetic substrate. This will allow the control of the film growth direction, via magnetic anisotropy, selective doping, and possibly even magnetic patterning.

In this work we study the behaviour of nickel and cobalt implanted in MgO. We use ion implantation to introduce a high concentration of ions into single crystals of MgO aiming at producing magnetic metallic precipitates. The ion implantation technique was chosen because it is a suitable doping technique that is not limited by thermodynamic constraints allowing the introduction of a specified amount of ions in a shallow region of the material. High fluence ion implantation frequently leads to the direct formation of aggregates and nanosized particles of the implanted ions in a wide class of materials. The influence of the implantation energy and of subsequent annealing treatment on the final system is analysed.

2 Experimental details

MgO single crystals grown by an arc-fusion technique [3] and cleaved in {100} orientation were implanted with fluences of 1×10^{17} cm^{-2} of either Co or Ni ions, with energies of 100 and 250 keV. A subsequent annealing treatment was carried out in vacuum, in two steps of one hour, at 1073 and 1273 K, to promote lattice recovery and diffusion of the implanted ions. In the following figures and tables, the MgO samples will be referred to by the symbol of the implanted ion followed by the implantation energy in keV, e.g. Co250 refers to a single crystal implanted with cobalt ions at 250 keV. Suffixes AsI and Ann refer to as-implanted and annealed samples, respectively.

Rutherford backscattering spectrometry (RBS), and RBS in combination with the channelling effect (RBS-C), performed with a 2 MeV He^+ beam, were used to characterize the depth profiles of the implanted species as well as the recovery behaviour of the host lattice before and after the annealing treatment.

[a] e-mail: mmcruz@fc.ul.pt

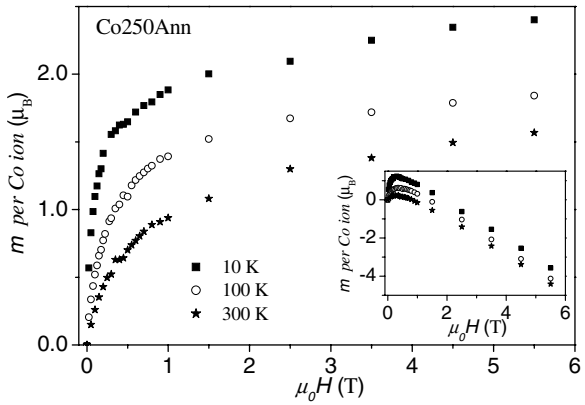

Fig. 1. Isothermal curves of the variation of the magnetic moments with the applied field for the Co250Ann sample. The main graphic displays the experimental magnetic moments after subtracting the diamagnetic contribution, while the inset displays the experimental results before this operation.

To characterize the magnetic behaviour of the samples, magnetic moment measurements were made using a Quantum Design MPMS magnetometer, for applied magnetic fields up to 5.5 T and temperatures between 2 and 400 K. For all implanted samples, the magnetic moment results are interpreted as the sum of two independent components: a diamagnetic contribution assigned to the unimplanted MgO matrix, and the contribution of the implanted region. From the characterization of several unimplanted crystals the magnetic susceptibility of MgO was determined to be -4.9×10^{-9} m^3/kg. Since the implanted region is only a very small fraction of the total sample volume ($\ll$0.1 %), the diamagnetic contribution was subtracted in all the experimental data presented. Figure 1 illustrates the isothermal magnetic moment data before and after this subtraction.

3 Experimental results

For the same energy of implantation, samples implanted with either Co or Ni ions yield similar results. Table 1 summarizes the profiles parameters obtained from the RBS and RBS-C measurements. A comparison of the 250 keV and 100 keV implantations shows that the former leave the implanted ions at depths that extend for 500 nm, with maximum atomic concentration of 4.5 at.%, for both Co and Ni, while the latter leave the ions at shallower depths (≈250 nm) with maximum concentrations of the order of 15 at.%. In the case of the 100 keV implantations, although the nominal values were identical, the retained fluence of Ni is higher by 20 % than that of Co, thereby explaining the differences found in the local maximum concentrations. A large amount of defects and the consequent amorphization of the implanted region was deduced from the RBS-C measurements and attributed to the high fluence implanted. After the annealing, there was no significant modification of the depth profiles of the implanted ions and only a marginal recovery of the host lattice structure was detected. No correlation was found between the location of the implanted ions and the structure of the host lattice, both in the as-implanted samples and after annealing.

Table 1. Depth profile parameters for the implanted ions, obtained by RBS spectrometry: maximum concentrations (c_{max}), depth of maximum (d_{cmax}) and maximum range (d_{max}).

Sample	*Retained fluence* (ions/cm^2)	c_{max} (at.%)	d_{cmax} (nm)	d_{max} (nm)
Co100	0.96×10^{17}	13	50	270
Co250	0.95×10^{17}	4.5	95	500
Ni100	1.20×10^{17}	18	60	250
Ni250	0.98×10^{17}	4.5	100	500

Previous experimental results indicate that there is a clear correlation between the magnetic behaviour and the concentration of the implanted ions [4]. For this reason, the results will be grouped and discussed according to the implantation energy. Since the implantations with higher energies result in lower local concentrations, this case will be discussed first.

3.1 250 keV implantation

The results of Zero Field Cooled/Field Cooled (ZFC/FC) measurements of the magnetic moment versus temperature for MgO crystals implanted with either Ni or Co ions are presented in Figure 2. In both cases a Curie law fits the temperature dependence of the experimental data.

In nickel implanted MgO, assuming that all Ni ions are paramagnetic, the magnetic moment per Ni ion obtained from the Curie constant is 3.8 μ_B. This value is comparable with the magnetic moment of free Ni ions and consistent with the presence of diluted ions.

For MgO implanted with cobalt, the temperature dependence can also be described with a paramagnetic Curie type behaviour, but added to a positive and temperature independent magnetic moment. The magnetic moment deduced from the Curie constant is 8.0 μ_B per Co ion, even higher than the Co^{2+} non-quenched ionic moment, indicating that some aggregation of the implanted ions may already exist. The temperature independent magnetic moment is attributed to the presence of ferromagnetic aggregates which represent a fraction of cobalt ions not larger than 1%.

The results obtained after annealing are displayed in Figure 3. For both implanted species, the temperature dependence of the magnetic moment can still be described by a Curie law, but with too high values of the magnetic moment per implanted ion (≈30–60 μ_B), indicating that it cannot be explained through the paramagnetic response of individual ions. This behaviour, together with the detection of a maximum in the $m(T)$ ZFC curves at low field (indicating the existence of a blocking temperature), is one finger print of the presence of superparamagnetic aggregates [5]. The blocking temperatures, T_B, determined

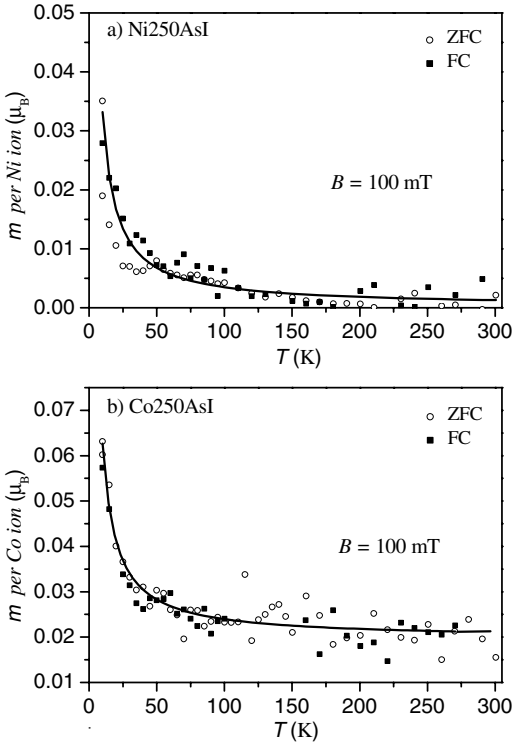

Fig. 2. Magnetic moment versus temperature obtained at 100 mT for a) Ni250AsI and b) Co250AsI. The solid lines are the fitted Curie laws.

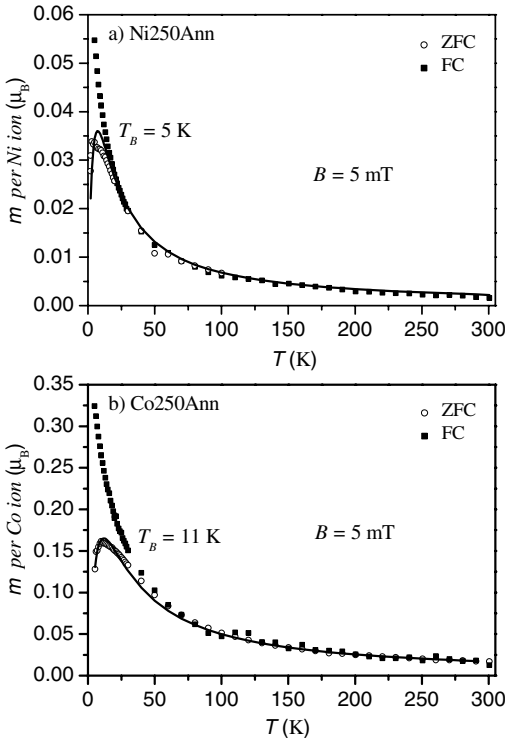

Fig. 3. ZFC/FC magnetic moment data at 5 mT: a) Ni250Ann and b) Co250Ann. The solid lines represent the theoretical fit to ZFC data.

from the position of the maxima, are 5 K and 11 K, for Ni and Co respectively. Measurements of the magnetic moment as a function of applied field are consistent with the existence of metallic nanosized aggregates of these ions: above T_B, the isotherms display no hysteresis and scale with H/T (Fig. 4), whereas below T_B, hysteresis exists (Fig. 5). Coercive fields of 13 mT, for nickel at 2 K, and 32 mT for cobalt at 3 K are derived.

The dependence of the magnetic moments with the applied field (Fig. 4) can be described by one component that is linear with the applied field and another that saturates. It is this latter component that is associated with the presence of metallic nanosized aggregates.

The saturation moment measured at 10 K in the Co implanted sample (not shown in Fig. 4) increases from 0.6 μ_B/Co-ion in the as-implanted state to 1.8 μ_B/Co-ion after annealing, indicating that all cobalt ions become associated in metallic aggregates (the saturation moments are 1.72 μ_B/Co-ion and 1.75 μ_B/Co-ion for the hcp and fcc metals, respectively). For the nickel implanted sample, the measured saturation moment is 0.25 μ_B/Ni-ion after annealing, and corresponds to 40 % of the Ni ions in metallic aggregates (the saturation moment of Ni fcc metal is 0.62 μ_B/Ni-ion).

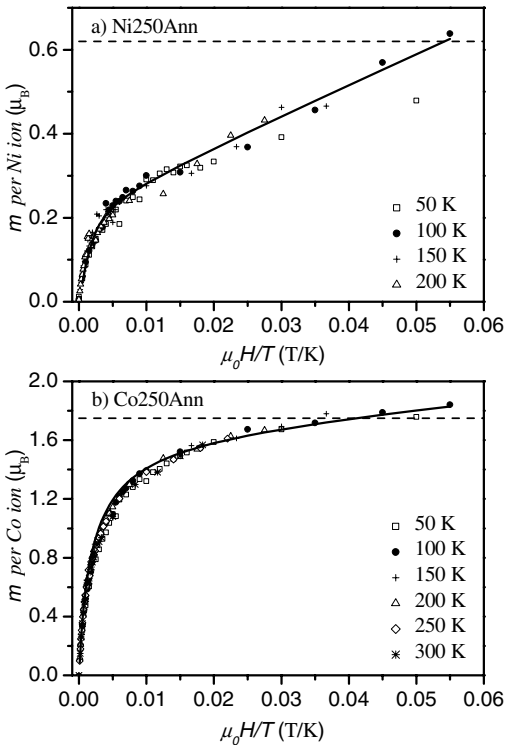

Fig. 4. Isothermal magnetic moments plotted as a function of $\mu_0 H/T$ for a) Ni250Ann and b) Co250Ann. The solid lines represent the fitted Langevin function added with a linear component. The dashed lines indicate the magnetic moment values in the fcc ferromagnetic metals, $0.62\mu_B$/Ni-ion and $1.75\mu_B$/Co-ion.

3.2 100 keV implantation

The results of a similar set of measurements for the case of 100 keV implantations are displayed in Figures 6 through 8.

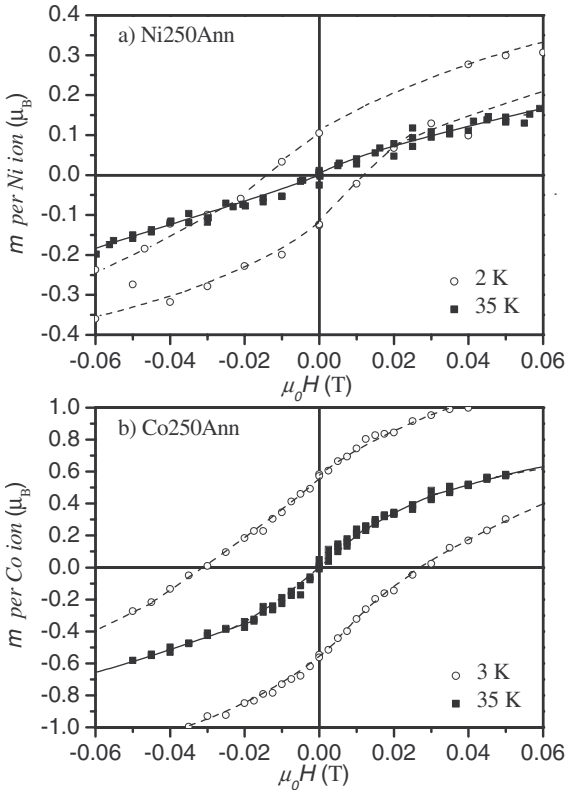

Fig. 5. Hysteresis data taken below and above the blocking temperature for the annealed samples: a) Ni250Ann and b) Co250Ann. The lines are drawn to guide the eye.

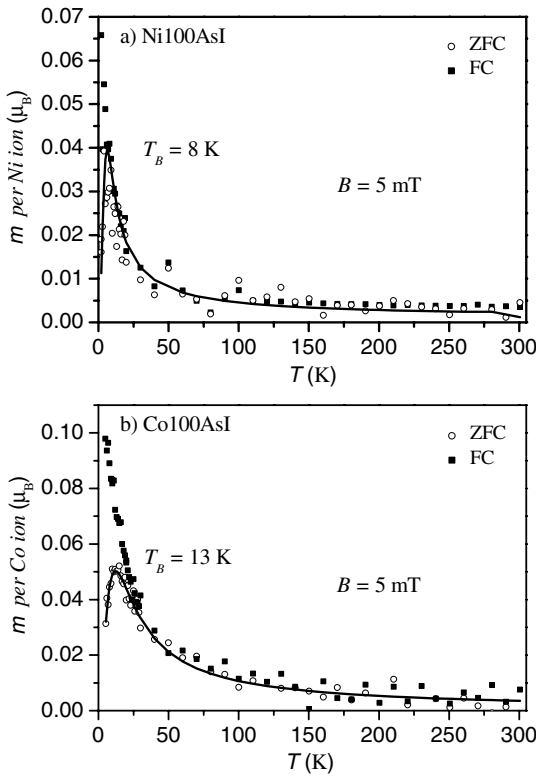

Fig. 6. ZFC/FC magnetic moment data at 5 mT: a) Ni100AsI and b) Co100AsI. The solid lines represent the theoretical fit to ZFC data.

The temperature dependence of the ZFC/FC magnetic moment obtained for Ni and Co as-implanted MgO are presented in Figure 6. Both systems already exhibit the superparamagnetic behaviour associated with the presence of nanosized magnetic aggregates, together with a paramagnetic contribution attributed to diluted ions. Blocking temperatures were found to be 8 K and 13 K for Ni and Co respectively. Accordingly, hysteresis exists below the blocking temperatures and disappears above. The coercive fields obtained for Ni and Co are 22 mT ($T = 2$ K) and 75 mT ($T = 3$ K), respectively.

After annealing, important modifications are detected in the magnetic behaviour of these 100 keV implanted MgO crystals. As the data displayed in Figures 7 and 8 show, the behaviour is still essentially superparamagnetic. However, there is a marked increase of the average magnetic moment of the aggregates, evidenced by the displacement of the blocking temperatures to higher values: 125 K for Ni and above 300 K for Co samples (Fig. 7). This displacement can be explained by the growth of the metallic aggregates. Furthermore, the asymptotic values of $m(T)$ are positive and can be accounted for by the presence of larger aggregates with T_B above the highest temperatures achieved experimentally.

The fraction of implanted ions in aggregates becomes nearly 100% in both cases.

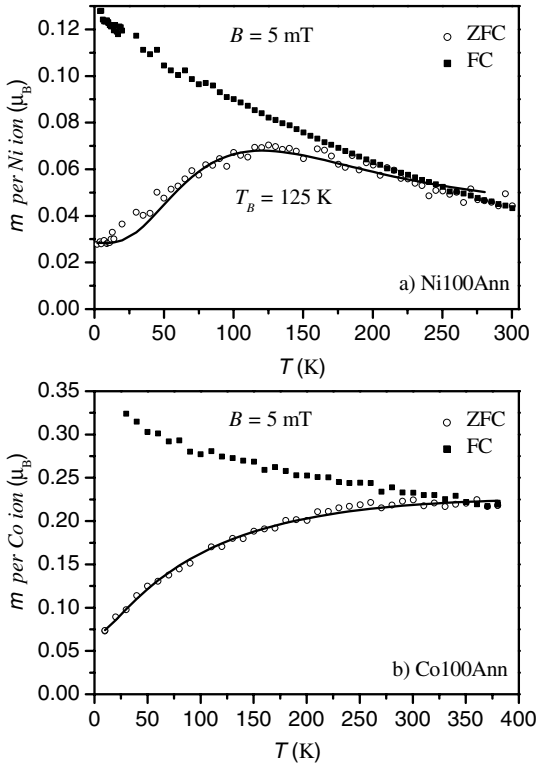

Fig. 7. ZFC/FC magnetic moment data at 5 mT: a) Ni100Ann and b) Co100Ann. The solid lines represent the theoretical fit to ZFC data.

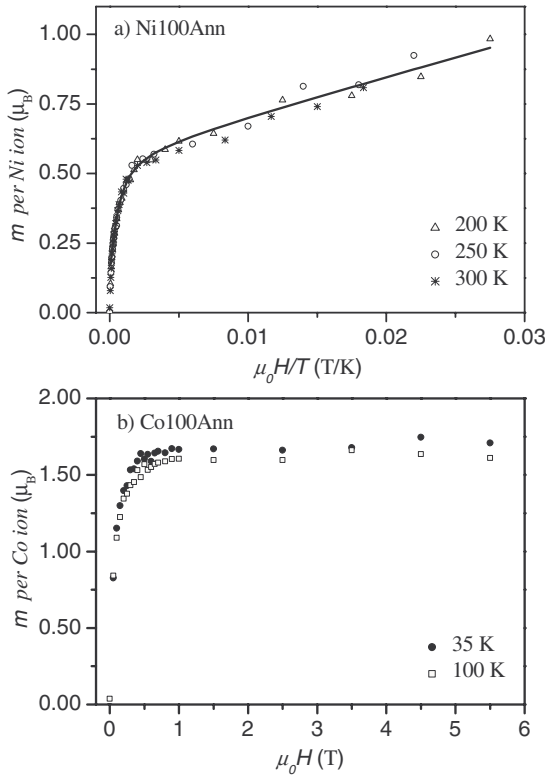

Fig. 8. a) Isothermal magnetic moment plotted as a function of $\mu_0 H/T$ for Ni100Ann. b) Isothermal magnetic moment as a function of $\mu_0 H$ for Co100Ann. Since no measurements above T_B were possible for this system the H/T scaling regime was not accessed.

4 Discussion

The results presented in the previous section show that Co and Ni ions implanted into MgO single crystals form aggregates, their sizes being controlled by the local implanted concentration. In the case of the 250 keV implanted samples, the formation of nanoscale aggregates is only clear after the crystals were subjected to the thermal annealing. For the 100 keV implanted samples, the presence of aggregates was already detected after implantation, indicating that the higher local concentrations are sufficient to promote aggregation.

To characterize these nanoclusters, namely their size distributions, magnetic anisotropy and fractions of incorporated ions, the magnetic results were analysed by combining the field and temperature dependence of the magnetic moments.

In the paramagnetic regime, a scaling of the magnetic moment, m, with H/T is expected when considering isothermals $m(H)$ measured at different temperatures. Since m takes large values, a Langevin model was used to fit the experimental results. This model was weighed by a log-normal moment distribution [6] to account for the aggregate size distributions (the theoretical fit curves are displayed as solid lines superimposed on the experimental data in Figs. 4 and 8). The log-normal distribution reproduces our experimental results better than a symmetric one and implies a larger number of smaller moments when compared with the average magnetic moment. Since the magnetic field dependence is very sensitive to the distribution of magnetic moments, this fit was used to determine the standard deviation σ of the log-normal distribution and the median of the magnetic moments distribution, m_o. These parameters were then introduced in the theoretical function used to fit the experimental ZFC temperature dependence to obtain the effective magnetic anisotropy constant (see the Appendix). The corresponding theoretical fits are shown superimposed on the experimental results as solid lines (cf. Figs. 3, 6 and 7). Above the blocking temperature T_B, the superparamagnetic aggregates were assumed to have a magnetic susceptibility that follows a Curie-Weiss law, $\chi = C/(T+\theta)$. In every case, whenever θ was left as a free parameter, its value always became very close to zero, indicating that the interactions between aggregates are very weak. Consequently the θ-values were always set to zero in the final fits. Below T_B the blocked aggregates are assumed to contribute with the initial susceptibility of magnetic domains [7], considering a cubic structure with negative anisotropy constant K_1. This is the case for both Co and Ni fcc particles [8,9] (X-ray diffraction measurements in our samples showed that the structure of the Co particles is fcc [10], in agreement with other works [11,12]. Nickel fcc aggregates were also identified). The results of the theoretical fits are summarized in Table 2.

From the derived average magnetic moments $\langle m \rangle$, it is possible to determine a mean diameter d for the aggregates, considering the bulk density of each metal and assuming a spherical shape. These values are also presented in Table 2 and indicate that the dimensions of our magnetic aggregates range from 2 to 7 nm in diameter, i.e. they are indeed magnetic nanoparticles.

The anisotropy constants, K_{eff}, of the nanoparticles, derived from the fits, can be discussed in comparison with the values expected for bulk fcc Co and Ni. For cubic structures with negative K_1, the effective anisotropy constant for the superparamagnetic behaviour is given by [5] $K_{eff} = -K_1/12 - K_2/27$, and using the K_1 values published for Co [8] and Ni [9], $K_1(\mathrm{Co}) = -2.5\times10^5$ Jm^{-3} and $K_1(\mathrm{Ni}) = -1.2\times10^5$ Jm^{-3}, the resulting bulk values are $K_{eff}(\mathrm{Co}) \approx 2\times10^4$ Jm^{-3} and $K_{eff}(\mathrm{Ni}) \approx 1\times10^4$ Jm^{-3} in the low temperature range. Since no exact values of K_2 are available at these low temperatures and there are indications that they are smaller than K_1 [8,9], the corresponding contribution was neglected. Our experimental values obtained for K_{eff} are always significantly higher than the bulk values. This difference is expected as the surface anisotropy plays an important role in magnetic nanoparticles. Assuming that the bulk and surface anisotropy energies add independently and that the aggregates are approximately spherical with a diameter d, the anisotropy constant values should follow the relation:

$$K_{eff} = K_{bulk} + 6K_{surface}/d. \quad (1)$$

The results for the cobalt precipitates are well described by this dependence (Fig. 9), implying that $K_{surface}(\mathrm{Co}) \leq 0.1$ mJ/m^2 and $K_{bulk} = 2\times10^4$ Jm^{-3}.

Table 2. Experimental blocking temperatures and fitted parameters for the samples where superparamagnetic aggregates were identified. The symbol f stands for the fraction of implanted ions in aggregates, and K_{eff} represents the anisotropy constants of the aggregates. The mean magnetic moment $\langle m \rangle$ was calculated from m_0 (derived from the fit) using equation (A.4) given in Appendix. The mean diameter d was then calculated from this value, assuming metallic spherical aggregates.

Sample	T_B(K)	$m_0(\mu_B)$	σ	$f_{m(H/T)fit}$ (%)	$f_{m(T)fit}$ (%)	$K_{eff}(10^4 \mathrm{Jm}^{-3})$	$\langle m \rangle(\mu_B)$	d(nm)
Co250Ann	11	680	1.0	85	85	21	1121	2.4
Co100AsI	13	785	0.66	35	35	37	976	2.3
Co100Ann	>300	10000[a]	1.4	100[b]	100	18	26275	6.8
Ni250Ann	5	1600	1.0	33	14	2.0	2638	4.5
Ni100AsI	8	1700	0.5	45	20	4.1	1926	4.1
Ni100Ann	125	7000	0.65	75	70	18	8647	6.7

[a] In this case the magnetic moment was derived only from the experimental temperature dependence
[b] Since no scaling with H/T exists below 380 K this fraction was derived using the saturated magnetic moment at 35 K

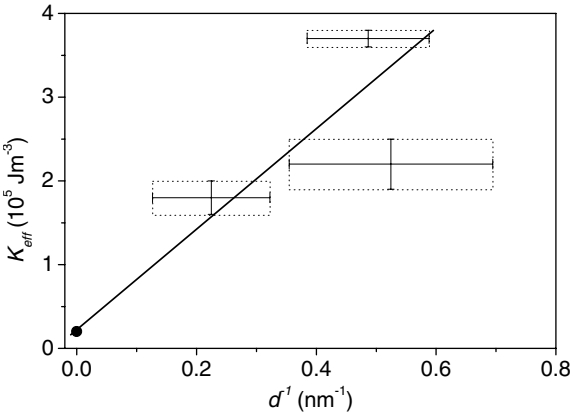

Fig. 9. Anisotropy constants as a function of the inverse diameter of the Co particles. The full symbol refers to the bulk metal.

The surface anisotropy constant is to be compared with the experimental value of 0.33 mJ/m^2, obtained for cobalt particles in Al_2O_3 [12,13]. This difference can be attributed to the particle shape, the lower value found in our case indicating that particles are highly symmetric in MgO.

In the case of nickel precipitates the experimental value of the anisotropy constant is higher for the larger particles (see Tab. 2), indicating that factors other than the surface anisotropy are more important. To confirm how the magnetic anisotropy constant values change with particle size, we also estimated these parameters using the temperature dependence of the coercive field below T_B. Assuming that the magnetic particles are randomly oriented and considering:

$$H_c = 0.52 K_{eff}/\mu_o M_{sat}(1 - (T/T_B)^n) \qquad (2)$$

with n having a value between 0.5 and 1 [5,14], the K_{eff} values presented in Table 3 were obtained. These calculated anisotropy constants are based only on two values of the coercive field determined for different and very large width distributions, but they corroborate the evolution of

Table 3. Blocking temperatures and effective anisotropy constants determined using equation (2).

Sample	T_B(K)	$K_{eff}(10^4$ Jm$^{-3})$
Co250Ann	11	10
Co100AsI	11	26
Co100Ann	300	5.4
Ni250Ann	13	1.1
Ni100AsI	10	2.0
Ni100Ann	110	2.7

the ZFC fit parameter K_{eff} with the aggregate size: it decreases with the size of the aggregates in Co implanted MgO and increases for Ni implanted MgO. This result implies that the anisotropy constant of nickel aggregates must have a different origin other than the surface. The possible formation of an oxide layer was investigated measuring the hysteresis curves in the blocked regime after lowering the temperature through T_B in a field of 5.5 T. The resulting hysteresis curves are asymmetric with respect to zero magnetic field, as illustrated in Figure 10. This is an indication of the presence of an antiferromagnetic layer surrounding the nickel aggregates, possibly a nickel oxide layer [11]. Such a layer can explain the anomalous behaviour of the anisotropy constants and also the general trend of the fitted fractions of nickel in nanosized aggregates: the fractions obtained from the temperature dependence fits are always lower than when derived from the field dependence fits. The non-saturating behaviour of the high field magnetic susceptibility $m(H)$ in the Ni implanted samples is also an indication of the presence of such an antiferromagnetic layer.

5 Conclusions

The experimental results presented show that ion implantation of Co or Ni into MgO single crystals results in the formation of magnetic nanoparticles of these ions. The number and size of these aggregates depend on the atomic concentration of the implanted ions and the subsequent annealing treatments. In the case of the 250 keV

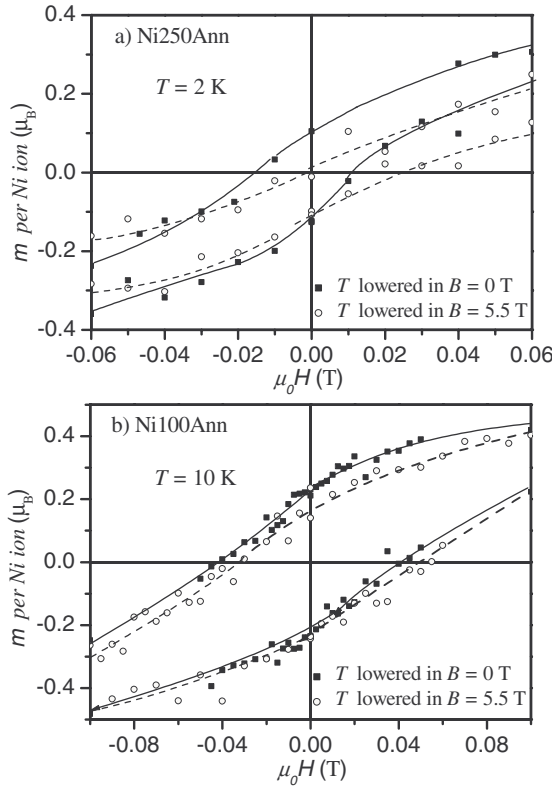

Fig. 10. Comparison of the hysteresis data taken below T_B for the Ni implanted samples after annealing: a) Ni250Ann and b) Ni100Ann. The lines are drawn to guide the eye.

implanted samples, the presence of nanosized aggregates is only identified after annealing at 1273 K. For the 100 keV implantations, aggregates are already detected in the as-implanted state. These differences can be explained on the basis of the higher local concentrations attained at lower implantation energies (for the same implantation fluences). The general behaviour of the so formed aggregates is superparamagnetic, indicating that these are single domain magnetic particles with average dimensions in the range of a few tens of nanometers. Particles sizes increase after annealing at 1273 K, and no detectable loss of the implanted ions was observed, showing that they are stable in MgO (the more diluted ions diffuse towards these particles and do not leave the crystal). From the characterization of the exhibited superparamagnetic behaviour, the anisotropy constants were derived. For cobalt aggregates, the dependence of these constants on the average size of the precipitates makes it possible to determine the surface anisotropy constant, and conclude that the aggregates must be more symmetric in MgO than in sapphire. For nickel aggregates, the behaviour of the anisotropy constant and hysteresis curve is attributed to the formation of an antiferromagnetic layer at the surface of the particles. No similar behaviour was detected in cobalt precipitates. This indicates that although the aggregation of metallic nickel and cobalt is similar, the interfaces between the aggregates and the MgO matrix are different.

Our results show that ion implantation of either Co or Ni into MgO is a suitable way to obtain magnetic nanoparticles with a controlled size distribution. By annealing, these particles grow and maintain their magnetic behaviour. This indicates that magnetic patterns can be drawn in MgO using Co or Ni implantations, with the added possibility of modulation of the size of the aggregates within the same sample, by using different implantation energies and fluences (to achieve the desired local concentration levels), and/or different local thermal treatments. The study of the stability of the magnetic aggregates subjected to further annealing treatments is in progress.

This work was partially supported by the Portuguese Foundation for Science and Technology, FCT, through the Ph.D. grant BD/8907/2002 to J.V. Pinto. It is part of a joint research program between ITN, Univ. Nova de Lisboa and the CFMC-FCUL of the University of Lisboa, in Portugal, with support of CRUP grant AI-E88/04, and the University Carlos III, of Madrid, supported by the CICYT of Spain under contract MAT 2002-01870 and HP 2003-0009. We are indebted to Y. Chen for providing the MgO crystals

Appendix

The magnetic moment of each sample is calculated using:

$$m(T) = \mu_o f m_s \times \frac{\frac{H}{3k_B(T+\theta)} \int_0^{\mu_T} \mu^2 P(\mu) d\mu + \frac{M_s H}{2|K_1|} \int_{\mu_T}^{\infty} \mu P(\mu) d\mu}{\int_0^{\infty} \mu P(\mu) d\mu} \quad \text{(A.1)}$$

where μ_o is the magnetic permeability, f is the fraction of the implanted ions in aggregates, $m_s = M_s V$ is the sample saturation moment, H is the external magnetic field and M_s the metal saturation magnetisation, K_{eff} is the effective magnetic anisotropy constant, K_1 is the usual anisotropy constant parameter, considered dependent of K_{eff} through $|K_1| = 12K_{eff}$ and $P(\mu)$ stands for the log-normal distribution. The integration variable μ represents the magnetic moment of the individual aggregates. The integration limit $\mu_T = 30k_BTM_s/K_{eff}$ is the magnetic moment that separates blocked from non-blocked aggregates at each temperature. This cut-off value is determined by the relaxation time of the particles, τ_0, which depends on the anisotropy energy barrier $K_{eff}V$ with V standing for the particle volume and K_{eff} for the effective magnetic anisotropy constant:

$$k_BT \ln(t/\tau_0) = K_{eff}V = K_{eff}\mu/M_s \quad \text{(A.2)}$$

t is the characteristic time of the measurement, around 100 s, and the relaxation time is assumed of the order of 5×10^{-12} s, value obtained from relaxation measurements.

θ was assumed equal to zero in all final fits.

For nickel aggregates the temperature dependence of the anisotropy constant [9] was approximated by a linear dependence by taking $K_{eff}(T) = K_{eff}(1 - T/300)$ for

$T < 300$ K. The K_{eff} value obtained from the fit is the anisotropy constant in the low temperature limit.
The log-normal distribution used for the magnetic moments has the expression:

$$P(\mu)d\mu = \frac{1}{\sqrt{2\pi}\sigma} \exp[-\ln^2(\mu/m_0)/2\sigma^2]\frac{d\mu}{\mu}. \quad (A.3)$$

Here σ stands for the standard deviation of the normal distribution of the logarithm of the magnetic moments and m_0 is the median of the magnetic moment distribution. To obtain the average magnetic moment one must use the relation:

$$\langle m \rangle = m_0 \exp(\sigma^2/2). \quad (A.4)$$

References

1. Y. Matsumoto, M. Murakami, T. Shono, T. Hasegawa, T. Fukumura, M. Kawasaki, P. Ahmet, T. Chikyow, S. Koshihara, H. Koinuma, Science **854**, 291 (2001)
2. S.A. Chambers, T. Doubray, C.M. Wang, A.S. Lea, R.F.C. Farrow, L. Folks, V. Deline, S. Anders, Appl. Phys. Lett. **82**, 1257 (2003)
3. M.M Abraham, C.T. Butler, Y. Chen, J. Chem. Phys. **55**, 3752 (1971)
4. M.M. Cruz, R.C. da Silva, J.V. Pinto, R. Gonzalez, E. Alves, M. Godinho, J. Magn. Magn. Mater. **272-276**, 840 (2004)
5. J.L. Dormann, D. Fiorani, E. Tronc, Adv. Chem. Phys. **98**, 283 (1977)
6. N. Peleg, S. Shtrikman, G. Gorodetsky, IEEE Trans. Magn. **32**, 4675 (1996)
7. S. Chikazumi, *Physics of Magnetism* (John Wiley & Sons, 1964), Chap. 13
8. W. Sucksmith, J.E. Thompson, Proc. R. Soc. London, Ser. A **225**, 362 (1954)
9. E.P. Wolhlfarth, *Ferromagnetic Materials, Vol. I*, edited by E.P. Wolhlfarth (North-Holland, 1986), Chap. 1
10. N. Franco (private communication, 2004)
11. J.P. Chen, C.M. Sorensen, K.J. Klabunde, G.C. Hadjipanayis, Phys. Rev. B **51**, 11527 (1995)
12. F. Luis, J.M. Torres, L.M. Garcia, J. Bartolomé, J. Stankiewicz, F. Petroff, F. Fettar, J.-L. Maurice, A. Vaurés, Phys. Rev. B **65**, 094409-1 (2002)
13. J.M. Torres, F. Luis, L.M. Garcia, J. Bartolomé, J. Stankiewicz, F. Petroff, F. Fettar, A. Vaurés, J. Magn. Magn. Mater. **242-245**, 575 (2002)
14. A. Gonzalez, A. Hernando, Phys. Rev. B **65**, 094432-1 (2002)